Al Flux Synthesis of the Oxidation-Resistant Quaternary Phase $REFe_4Al_9Si_6$ (RE = Tb, Er)

Bradley Sieve,[†] Danielle L. Gray,[‡] Robert Henning,[§] Thomas Bakas,[||] Arthur J. Schultz,[§] and Mercouri G. Kanatzidis*[,‡]

Department of Chemistry, Northern Kentucky University, Highland Heights, Kentucky 41099, Department of Chemistry, Northwestern University, Evanston, Illinois 60208, Intense Pulsed Neutron Source, Argonne National Laboratory, Argonne, Illinois 60439, Department of Physics, University of Ioannina, Ioannina, 45110 Greece

Received June 9, 2008. Revised Manuscript Received July 22, 2008

Two rare earth iron aluminum silicides, $REFe_4Al_9Si_6$ (RE = Tb, Er), were synthesized in liquid Al at temperatures below 850 °C. They crystallize in the tetragonal space group $P4_2/nmc$ (no. 137) with cell dimensions of $a = 8.718(1)$ Å and $c = 15.171(3)$ Å for the Tb analogue. The structure, which is highly intricate and represents a rare structural arrangement, is based on that of $NdRh_4Al_{15.4}$. It can be understood in terms of highly corrugated layers of merged Al_6 rings stacking to form a three-dimensional framework. The Fe and Si atoms are situated in various sites in the framework. The RE atoms have a very high coordination number (20) and sit in remaining pockets formed by the bonding arrangements in the structure. Magnetic measurements show that the rare earth ions are in a 3+ state, whereas Mössbauer measurements show that the Fe atoms do not exhibit a magnetic moment and are more reduced than in elemental Fe. The possible insights gained from these results into the metallurgical processing of advanced aluminum matrix alloys are discussed. Thermal gravimetric analysis experiments in air show that $REFe_4Al_9Si_6$ is resistant to oxidation up to 900 °C, which is attributable to an alumina/silica surface scale.

Introduction

Metal silicides are technologically relevant because they are involved in diverse technology fields, such as silicon-based electronic devices, refractory electrode materials, advanced structural materials, amorphous metals, and aluminum matrix composites.[1−7] Silicide synthesis normally relies on direct combination of elemental reactants at very high temperatures, over 1500 °C. These temperatures require high-energy methods, such as induction heating and arc-melting. Although annealing or quenching can sometimes yield single crystals, generally they produce microcrystalline samples. The use of metallic fluxes as synthetic media presents significant synthetic advantages, such as solution-like conditions, lower reaction temperatures, facile crystal growth, and allowing the reaction system to "find its way" to the final product under the prevailing experimental conditions.[8] The latter is a particularly important point because most often in intermetallic chemistry, the product stoichiometry is so unusual and complex it cannot be predicted by any known rationale, be it conventional or state of the art. Arguably, exploratory synthesis utilizing such solution methods have generated many new Al/(Si or Ge)-containing compounds, including $Sm_2Ni(Si_{1-x},Ni_x)Al_4Si_6$,[9] $RENiAl_4Ge_2$ (RE = Sm, Tb, Y),[10] $RE_4Fe_{2+x}Al_{7-x}Si_8$ (RE = Ce, Pr, Nd, Sm),[11] $RE_8Ru_{12}Al_{49}Si_9(Al_xSi_{12-x})$ (RE = Sm and Pr),[12] $RE_2Al_3Si_2$ (RE = Ho, Er, Tm),[13] $Tb_2NiAl_4Ge_2$,[14] $REAu_3Al_7$,[15−17] $Co_5Al_{14}Si_2$,[18] and $Ce_2NiAl_{6-x}Ge_{4-y}$ ($x \sim$

* To whom correspondence should be addressed. E-mail: m-kanatzidis@northwestern.edu.
[†] Northern Kentucky University.
[‡] Northwestern University.
[§] Argonne National Laboratory.
[||] University of Ioannina.

(1) Reader, A. H.; Vanommen, A. H.; Weijs, P. J. W.; Wolters, R. A. M.; Oostra, D. J. *Rep. Prog. Phys.* **1993**, *56* (11), 1397–1467.
(2) Johnson, V.; Jeitschko, W. *J. Solid State Chem.* **1972**, *4* (1), 123.
(3) Rohatgi, P. *J. Miner. Met. Mater. Soc.* **1991**, *43* (4), 10–15.
(4) Suresh, S.; Mortensen, A.; Needleman, A. Butterworth-Heinemann: Stoneham, MA 1993.
(5) Nardone, V. C.; Strife, J. R.; Prewo, K. M. *Metall. Trans. A* **1991**, *22* (1), 171–182.
(6) McDanels, D. L. *Metall. Trans. A* **1985**, *16* (6), 1105–1115.
(7) Ma, Q.; Yan, B. J.; Kang, M. K.; Yang, Y. Q. *Rare Met. Mater. Eng.* **1999**, *28* (1), 10–13.
(8) Kanatzidis, M. G.; Pottgen, R.; Jeitschko, W. *Angew. Chem., Int. Ed.* **2005**, *44* (43), 6996–7023.
(9) Chen, X. Z.; Sportouch, S.; Sieve, B.; Brazis, P.; Kannewurf, C. R.; Cowen, J. A.; Patschke, R.; Kanatzidis, M. G. *Chem. Mater.* **1998**, *10* (10), 3202–3211.
(10) Sieve, B.; Chen, X.; Cowen, J.; Larson, P.; Mahanti, S. D.; Kanatzidis, M. G. *Chem. Mater.* **1999**, *11* (9), 2451–2455.
(11) Sieve, B.; Sportouch, S.; Chen, X. Z.; Cowen, J. A.; Brazis, P.; Kannewurf, C. R.; Papaefthymiou, V.; Kanatzidis, M. G. *Chem. Mater.* **2001**, *13* (2), 273–283.
(12) Sieve, B.; Chen, X. Z.; Henning, R.; Brazis, P.; Kannewurf, C. R.; Cowen, J. A.; Schultz, A. J.; Kanatzidis, M. G. *J. Am. Chem. Soc.* **2001**, *123* (29), 7040–7047.
(13) Chen, X. Z.; Sieve, B.; Henning, R.; Schultz, A. J.; Brazis, P.; Kannewurf, C. R.; Cowen, J. A.; Crosby, R.; Kanatzidis, M. G. *Angew. Chem. Int. Ed.* **1999**, *38* (5), 693–696.
(14) Sieve, B.; Trikalitis, P. N.; Kanatzidis, M. G. *Z. Anorg. Allg. Chem.* **2002**, *628* (7), 1568–1574.
(15) Wu, X. N.; Kanatzidis, M. G. *J. Solid State Chem.* **2005**, *178* (11), 3233–3242.
(16) Latturner, S. E.; Bilc, D.; Mahanti, S. D.; Kanatzidis, M. G. *Inorg. Chem.* **2003**, *42* (24), 7959–7966.
(17) Latturner, S. E.; Bilc, D.; Ireland, J. R.; Kannewurf, C. R.; Mahanti, S. D.; Kanatzidis, M. G. *J. Solid State Chem.* **2003**, *170* (1), 48–57.
(18) Wu, X. U.; Latturner, S.; Kanatzidis, M. G. *Inorg. Chem.* **2006**, *45* (14), 5358–5366.

10.1021/cm801554d CCC: $40.75
Published on Web 09/10/2008

0.24, $y \sim 1.34$).[14] The plethora of stoichiometric diversity is astonishing and underscores how little is known about how intermetallics become stabilized or what gives rise to the stoichiometries observed.

In addition to being of basic scientific interest, complex intermetallics of Al are important to applied metallurgy because of their relationships to aluminum matrix composites.[4] Many Al matrix composites contain other elements that react and form ternary or quaternary aluminide phases within the Al matrix, either during the initial preparation of the material or over time through use. These formed phases may be either beneficial to the properties of the alloys or detrimental, thus contributing to eventual failure. Detailed knowledge of these minor phases and their behavior can therefore be critical in understanding and designing better materials for the future. One example of the importance of complex multinary compounds forming within Al alloys is $Cu_2Mg_8Al_5Si_6$, which has been shown to significantly increase matrix strength without increasing the overall weight.[19−23] Two elements commonly found in Al-based alloys are Fe and Si.[24−27] Iron is one of the most troublesome impurities. During solidification, iron promotes the formation of intermediate phases that may degrade the mechanical properties of the final product.[28] Knowledge of the chemistry of iron in liquid aluminum in the presence of other elements, such as silicon, enhances the understanding of the fate of iron in these systems. This knowledge could help in the design of helpful ways to control iron precipitate and its effects on the alloy properties.

Oxidation-resistant intermetallics are of great interest in applications involving extreme environments; however, studies of the response of complex new materials toward high-temperature oxidation are relatively rare. Very few complex, single-crystalline systems have been studied for oxidation resistance. They include $RE_5Co_4Si_{14}$ (RE = Ho, Er, Tm, Yb),[29] $V_2Al_5Ge_5$,[30] $ErRh_3B$, $ErRb_3B_2$, $ErRh_4B_4$,[31] $REMn_2Si_2$ (RE = La, Ce, Pr, Nd, Sm, Gd),[32] $Co_5Al_{14}Si_2$,[18] Nb_5Sn_2Ga,[33] and $YRh_3B_xC_{1-x}$ (x = 0, 0.2, 0.4, 0.6 0.8, 1).[34] Oxidation onset temperatures range from relatively low values of 500 °C for $V_2Al_5Ge_5$ to high onset temperatures of 1030 °C for $ErRh_3B$. The oxidation resistance is judged not only by the onset temperature of oxidation but also by the resistance of the compound to continue to gain mass after the onset temperature. Often, it is difficult to compare this value because of the effects of the experimental environments on the oxidation rate.

Studies of quaternary iron/aluminum and iron/silicon intermetallic systems have been relatively scarce, mostly concentrating on pseudoternary compounds, such as $Sm_2Fe_{14-x}Co_xAl_3$[35] or the quasi-crystalline phases that form in alloys of Al/Cu/Co/Fe.[36] Recently, a true quaternary phase was published, $RE_4Fe_{2+x}Al_{7-x}Si_8$ (RE = Ce, Pr, Nd, Sm), which was synthesized using the Al flux method.[11] Here, we present a second quaternary phase, $REFe_4Al_9Si_6$ (RE = Tb, Er), that crystallizes as an ordered version of the $NdRh_4Al_{15.4}$ structure type.[37] The new compounds are only the second members of this unusual structural type. The magnetic properties and Mössbauer spectroscopic characterization of these compounds, which show that the Fe atoms in the structure do not carry a magnetic moment, are reported here. In addition, the remarkable high-temperature oxidation resistance in air of these compounds is described. To the best of our knowledge, this is the first time an air oxidation study of a complex quaternary aluminosilicide has been performed at high temperatures. The results are both surprising and revealing in that they point to the intriguing possibility that with increased compositional complexity (e.g., quaternaries) there is greater probability of achieving a more adhering complex oxide layer capable of protecting against oxidation.

Experimental Section

Synthesis. *Method 1 (Flux Synthesis).* In a N_2 filled glovebox, RE (RE= Tb (Cerac Inc., −40 mesh, 99.9%) or Er (Cerac Inc., −40 mesh, 99.9%)), Fe (Aldrich Chemical, fine powder, 99.99%), Al (Cerac Inc., −20 mesh, 99.5%), and Si (Cerac, −325 mesh, 99.96%) were mixed in a 1:4:20:6 ratio and placed inside Al_2O_3 crucibles. The crucibles were placed inside fused-silica tubes and flame-sealed under vacuum ($<10^{-4}$ Torr) then heated to 850 °C in 20 h and maintained there for 4 d. The samples were cooled to 500 °C in 3 d and then to 50 °C in 12 h. The crucibles were removed from the tubes and submerged into a 5 M NaOH solution to isolate the products from the excess Al matrix. This procedure yielded two types of products, silvery cubelike crystals and black polycrystalline powder, both of which were identified as $REFe_4Al_9Si_6$ (RE = Tb, Er) by comparison of experimental powder X-ray diffraction patterns to calculated patterns from the solved crystal structures. On the basis of RE metal, yields for this reaction were ∼90−95%.

(19) Matsuda, K.; Teguri, D.; Sato, T.; Uetani, Y.; Ikeno, S. *Mater. Trans.* **2007**, *48* (5), 967–974.
(20) Lopez, I. A.; Zepeda, C. M.; Reyes, J. G. G.; Flores, A. M.; Rodriguez, J. S.; Gomez, L. B. *Mater. Charact.* **2007**, *58* (6), 509–518.
(21) Wang, X.; Esmaeili, S.; Lloyd, D. J. *Metall. Mater. Trans., A* **2006**, *37A* (9), 2691–2699.
(22) Ravi, C.; Wolverton, C. *Metall. Mater. Trans., A* **2005**, *36A* (8), 2013–2023.
(23) MacKenzie, M.; Weatherly, G. C.; McComb, D. W.; Perovic, A.; Craven, A. J. *Electron Microsc. Anal.* **2001**, *2001*, 283–286.
(24) Tokuda, K.; Kumai, S.; Ishihara, A.; Suzuki, K. Influences of iron content and solidification rate on mechanical properties of 6022 base aluminum alloys In *Aluminium Alloys*, Trans Tech Publications: Zurich, 2006, Pts 1 and 2, Vol. 519−521; pp 1889−1894.
(25) Thirugnanam, A.; Sukumaran, K.; Raghukandan, K.; Pillai, U. T. S.; Pai, B. C. *Trans. Indian Inst. Met.* **2005**, *58* (5), 777–787.
(26) Chen, B. Q.; Chai, C. X.; Peng, J. B. *J. Wuhan Univ. Technol., Mater. Sci. Ed.* **2003**, *18* (1), 25–28.
(27) Caceres, C. H.; Svensson, I. L.; Taylor, J. A. *Int. J. Cast Met. Res.* **2003**, *15* (5), 531–543.
(28) Dehmas, M.; Valdes, R.; Lafont, M. C.; Lacaze, J.; Viguier, B. *Scr.−Mater.* **2006**, *55* (2), 191–194.
(29) Salvador, J. R.; Malliakas, C.; Gour, J. R.; Kanatzidis, M. G. *Chem. Mater.* **2005**, *17*, 1636–1645.
(30) Wu, X.; Bilc, D.; Mahanti, S. D.; Kanatzidis, M. G. *Chem. Commun.* **2004**, 1506–1507.
(31) Shishido, T.; Kudou, K.; Okada, S.; Ye, J.; Oku, M.; Horiuchi, H.; Fukuda, T. *J. Alloys Compd.* **1998**, *280*, 65–70.
(32) Okada, S.; Iizumi, K.; Mori, T.; Shishido, T.; Kudou, K.; Tanaka, T.; Rogl, P.; Lundstrom, T. *J. Alloys Compd.* **2004**, *383*, 254–258.
(33) Okada, S.; Kudou, K.; Shishido, T.; Higashi, I.; Horiuchi, H.; Fukuda, T. *J. Alloys Compd.* **1998**, *281*, 160–162.
(34) Shishido, T.; Ye, J.; Okada, S.; Kudou, K.; Iizumi, K.; Oku, M.; Ishizawa, Y.; Amano, T.; Kohiki, S.; Kawazoe, Y.; Nakajima, K. *J. Alloys Compd.* **2003**, *354*, 198–201.
(35) Wang, Z.; Dunlap, R. A.; Foldeaki, M. *J. Mater. Sci.* **1994**, *29* (20), 5333–5336.
(36) Perez, R.; Juarezislas, J. A.; Martinez, L. *Mater. Sci. Eng., A* **1994**, *182*, 837–840.
(37) Fehrmann, B.; Jeitschko, W. *J. Alloys Compd.* **2000**, *298* (1−2), 153–159.

Table 1. Crystallographic Data and Refinement Details for $REFe_4Al_9Si_6$ (RE = Tb, Er)

formula	$TbFe_4Al_9Si_6$	$TbFe_4Al_9Si_6$	$ErFe_4Al_9Si_6$
radiation	Mo Kα (λ = 0.710 69 Å)	neutron (λ = 0.7−4.2 Å)	Mo Kα (λ = 0.710 69 Å)
formula wt	793.69	793.69	802.02
temp (K)	293(2)	298	293(2)
space group	$P4_2/nmc$	$P4_2/nmc$	$P4_2/nmc$
crystal size (mm)	0.04 × 0.03 × 0.03	1.0 × 2.5 × 3.0	0.30 × 0.23 × 0.17
unit cell dimensions (Å)	a = 8.7184(11)	a = 8.7184(11)	a = 8.6882(12)
	c = 15.171(3)	c = 15.171(3)	c = 15.115(3)
vol (Å^3)	1153.1(3)	1153.1(3)	1141.0(3)
μ (mm^{-1})	12.238	0.279 + 0.071·λ	13.525
θ range (°)	2.69−28.30	TOF Lauer with position-sensitive area detector	4.28−31.08
index ranges	$-11 \le h \le 11$	$-2 \le h \le 12$	$-12 \le h' 12$
	$-11 \le k \le 11$	$-4 \le k \le 12$	$-11 \le k \le 12$
	$-20 \le l \le 19$	$-2 \le l \le 21$	$-21 \le l \le 21$
reflections collected	10 686	2207	12 800
unique reflections	812	885	1001
data/restraints/parameters	812/0/60	885/0/59	1001/0/60
goodness-of-fit on F^2	1.273	1.046	1.351
final R indices [$I > 2\sigma(I)$]	R(F) = 0.0202	R(F) = 0.0401	R(F) = 0.0255
	$R_w(F^2)$ = 0.0505	$R_w(F^2)$ = 0.0915	$R_w(F^2)$ = 0.0656
R indices (all data)	R(F) = 0.0219	R(F) = 0.0493	R(F) = 0.0256
	$R_w(F^2)$ = 0.0510	$R_w(F^2)$ = 0.0959	$R_w(F^2)$ = 0.0657
largest diff. peak and hole (e$^-$/Å^3)	1.362, −0.685	1.147, −0.688	0.943, −1.096

$R(\mathrm{F}) = \sum ||F_0| - |F_c||/\sum |F_0|$ and $R_w(F^2) = [\sum (|F_0^2 - F_c^2|)^2/\sum (wF_0^2)^2]^{1/2}$.

Method 2 (Arc-Melting). In a N_2 filled glovebox, Tb, Fe, Al, and Si powders were mixed in a 1:4:20:6 atomic ratio. The mixtures were cold-pressed, loaded into an arc welder, and melted on a water-cooled Cu plate with a Zr-gettered Ar atmosphere for ∼30 s until a good melt was observed. The samples were then flipped and remelted several times to ensure homogeneity. The excess Al was then removed by submersion of the arc-melted pellets into a 5 M NaOH solution for 24 h. After the isolation, an X-ray powder diffraction pattern was acquired and was found to match the calculated pattern. Yields based on Tb metal for this reaction were on the order of 60%. Attempts to form this phase using stoichiometric amounts of the elements (i.e., without the excess Al present) were unsuccessful.

Microprobe Analysis. Semiquantitative microprobe analyses of $REFe_4Al_9Si_6$ (RE = Tb, Er) were performed with a JEOL JSM-6400 scanning electron microscope (SEM) equipped with a Noran Vantage energy disperse spectroscopy (EDS) detector. Data were acquired using an accelerating voltage of 25 keV with a 100 s accumulation time. Standards were recorded under the same experimental conditions to yield correction factors. After calibration, the title compounds gave elemental ratios of about "$REFe_{3.5}Al_9Si_7$" (for both analogues), which agrees well with the values from the refined X-ray structures. Crystals selected from the different synthetic methods were analyzed and showed no significant differences in elemental ratio. A Hitachi S3400N-II SEM equipped with an integrated Oxford EDS system was also used for imaging and semiquantitative microprobe analysis of crystals before and after the thermal gravimetric analysis experiments.

X-ray Crystallography. Single-crystal X-ray diffraction data for $REFe_4Al_9Si_6$ (RE = Tb, Er) were collected at 298 K on a Siemens Platform CCD diffractometer on using Mo Kα (λ = 0.71069 Å) radiation. SMART software (Data Collection Software for the SMART System, Siemens Analytical X-Ray Instruments Inc.) was used for the data acquisition, and the program SAINT[38] was used for the data extraction and reduction. An empirical absorption correction was applied to the data using SADABS, and the structures were solved with direct methods in the SHELXL package of programs. The crystallographic and refinement data are listed in Table 1. The fractional atomic coordinates and anisotropic displacement parameters (U^{ij} values) are listed in Tables 2 and 3, respectively.

Table 2. Atomic Coordinates (×10^4) for $REFe_4Al_9Si_6$ (RE = Tb, Er)[a]

	Wykoff position	x	y	z
Tb (X-ray)	4d	2500	2500	1642(1)
Tb (neutron)		2500	2500	1644(1)
Er		2500	2500	1641(1)
Fe(1)	8g	2500	4768(1)	−4(1)
		2500	4768(1)	−3(1)
		2500	4760(1)	−1(1)
Fe(2)	8f	5006(1)	4994(1)	2500
		5003(1)	4997(1)	2500
		5010(1)	4990(1)	2500
Al(1)	16h	655(1)	2500	3388(1)
		646(3)	2500	3391(1)
		656(2)	2500	3387(1)
Al(2)	8g	5019(1)	4553(1)	813(1)
		5017(2)	4568(2)	814(1)
		5024(2)	4536(2)	812(1)
Al(3)	8g	952(1)	7500	3503(1)
		954(3)	7500	3498(1)
		950(2)	7500	3505(1)
Al(4)	4c	2500	7500	−199(1)
		2500	7500	−193(2)
		2500	7500	−200(2)
Si(1)	8g	5939(1)	2500	1922(1)
		5937(2)	2500	1925(1)
		5938(2)	2500	1925(1)
Si(2)	8g	2500	4880(1)	3125(1)
		2500	4878(2)	3122(1)
		2500	4879(2)	3122(1)
Si(3)	8g	3878(1)	2500	−282(1)
		3871(3)	2500	−279(1)
		3877(2)	2500	−284(1)

[a] Note: Each first line is for X-ray analysis of $TbFe_4Al_9Si_6$; each second line is for the neuron analysis of $TbFe_4Al_9Si_6$; and finally, each third line is for the X-ray analysis of $ErFe_4Al_9Si_6$.

Neutron Diffraction. Before the structure of the compounds can be examined in any detail, a short discussion of the assignments of Al and Si atoms is required. Initial assignments of the atomic positions were made through analysis of the bond distances involving the particular atomic position. This approach is largely successful because of the significantly different size of Al and Si atoms. The assignments based on the bonding analysis placed Si

(38) SAINT. Data Processing Software for SMART System. Siemens Analytical X-Ray Instruments Inc., 1995.

Table 3. Anisotropic Displacement Parameters ($Å^2 \times 10^3$)[a] for $REFe_4Al_9Si_6$ (RE = Tb, Er)[b]

	U11	U22	U33	U23	U13	U12
Tb (X-ray)	13(1)	12(1)	9(1)	0	0	0
Tb (neutron)	5(1)	5(1)	6(1)	0	0	0
Er	22(1)	21(1)	16(1)	0	0	0
Fe(1)	14(1)	16(1)	9(1)	−1(1)	0	0
	7(1)	9(1)	6(1)	−1(1)	0	0
	22(1)	23(1)	15(1)	−1(1)	0	0
Fe(2)	12(1)	12(1)	10(1)	0(1)	0(1)	0(1)
	5(1)	5(1)	8(1)	0(1)	0(1)	0(1)
	21(1)	21(1)	16(1)	0(1)	0(1)	0(1)
Al(1)	16(1)	14(1)	10(1)	0	1(1)	0
	13(1)	6(1)	8(1)	0	−1(1)	0
	25(1)	23(1)	16(1)	0	1(1)	0
Al(2)	14(1)	20(1)	9(1)	2(1)	−1(1)	−3(1)
	9(1)	15(1)	8(1)	3(1)	−2(1)	−5(1)
	23(1)	28(1)	16(1)	2(1)	−1(1)	−3(1)
Al(3)	13(1)	18(1)	12(1)	0	1(1)	0
	6(1)	12(1)	12(1)	0	0(1)	0
	22(1)	27(1)	18(1)	0	1(1)	0
Al(4)	21(1)	15(1)	19(1)	0	0	0
	19(2)	9(1)	20(2)	0	0	0
	31(1)	22(1)	24(1)	0	0	0
Si(1)	18(1)	15(1)	16(1)	0	−3(1)	0
	13(1)	7(1)	17(1)	0	−5(1)	0
	26(1)	23(1)	22(1)	0	−2(1)	0
Si(2)	13(1)	15(1)	11(1)	0(1)	0	0
	4(1)	9(1)	11(1)	0(1)	0	0
	22(1)	23(1)	18(1)	0(1)	0	0
Si(3)	22(1)	14(1)	13(1)	0	1(1)	0
	19(1)	7(1)	14(1)	0	−1(1)	0
	28(1)	23(1)	20(1)	0	2(1)	0

[a] The anisotropic displacement factor exponent takes the form $-2\pi^2[h^2a^{*2}U11 + ... + 2hka^*b^*U12]$. [b] Note: Each first line is for X-ray analysis of $TbFe_4Al_9Si_6$; each second line is for the neuron analysis of $TbFe_4Al_9Si_6$; and finally, each third line is for the X-ray analysis of $ErFe_4Al_9Si_6$.

atoms in three 8g positions and Al atoms in a 16h and two 8g positions. One position that was troublesome was the 4c site. This position exhibited a distance of 2.4005(7) Å, which would correspond to a Si−Fe bond; however, all of the other bonding distances corresponded better to an Al atom in the position and not Si. To resolve the question of assignments, neutron diffraction was conducted on selected single crystals of $TbFe_4Al_9Si_6$. The neutron refinement confirmed the initial assignment of all atomic positions made on the basis of the X-ray refinement, except for the questionable 4c position. For this site, the neutron refinement proved critical because it clearly indicated Al at this position.

A single crystal of $TbFe_4Al_9Si_6$ (1.0 × 2.5 × 3.0 mm) was mounted on an aluminum pin and placed on the SCD diffractometer at the Intense Pulsed Neutron Source (IPNS) at Argonne National Laboratory. Time-of-flight Laue diffraction data with a wavelength of 0.7−4.2 Å were collected at room temperature on a position-sensitive area detector. At least one octant of reciprocal space was collected at 16 different angular settings of the crystal. The details of the data collection and analysis procedures have been described previously. An autoindexing routine was used to obtain an orientation matrix, and integrated intensities were corrected for the Lorentz factor and incident spectrum. A wavelength-dependent spherical absorption correction was applied, but symmetry-related reflections were not averaged because extinction is strongly wavelength-dependent. The structural refinement was performed using the GSAS program.[10] The crystallographic and refinement data are listed in Table 1. The fractional atomic coordinates, anisotropic displacement parameters (U^{ij} values), and selected bond distances are listed in Tables 2, 3, and 4 respectively.

Magnetic Susceptibility Measurements. Although single crystals were selected for the magnetic studies, a small magnetic impurity was present on the crystals, likely as powder on the surface,

Table 4. Bond Distances (Å) for $TbFe_4Al_9Si_6$ from Neutron Refinement

Tb−Al(3)	3.019(2)	Al(1)−Si(2)	2.660(2)
Tb−Si(1)	3.027(2)	Al(1)−Al(2)	2.651(2)
Tb−Al(1)	3.104(2)	Al(1)−Si(3)	2.849(3)
Tb−Al(2)	3.1066(17)	Al(2)−Si(1)	2.596(2)
Tb−Si(2)	3.054(2)	Al(2)−Al(2)	2.581(3)
Fe(1)−Si(3)	2.3482(14)	Al(2)−Si(3)	2.645(2)
Fe(1)−Al(4)	2.3994(10)	Al(2)−Si(3)	2.852(2)
Fe(1)−Al(1)	2.464(2)	Al(2)−Al(4)	2.971(2)
Fe(1)−Al(3)	2.505(2)	Al(3)−Si(2)	2.632(3)
Fe(1)−Al(2)	2.5255(16)	Al(3)−Al(3)	2.696(5)
Fe(1)−Al(2)	2.5567(16)	Al(3)−Si(2)	2.715(2)
Fe(2)−Si(2)	2.3802(9)	Al(3)−Al(2)	2.714(2)
Fe(2)−Si(1)	2.4824(12)	Al(3)−Al(4)	2.902(4)
Fe(2)−Al(2)	2.5855(16)	Al(4)−Si(1)	2.960(4)
Fe(2)−Al(1)	2.6238(13)	Si(1)−Si(1)	2.599(3)
Fe(2)−Al(3)	2.7847(15)	Si(1)−Si(1)	2.725(4)
Fe(2)−Tb	3.3450(6)	Si(2)−Si(3)	2.580(3)
Al(1)−Si(1)	2.617(3)	Si(3)−Si(3)	2.391(5)

although not seen by any other analysis method. To remove this impurity, the crystals were sonicated for 1 min in a 10% HCl solution. Magnetic susceptibility for $REFe_4Al_9Si_6$ (RE = Er, Tb) were measured as a function of both temperature and field using a Quantum Design MPMS SQUID magnetometer. An initial study of field dependence was conducted to find a suitable field for the variable temperature studies. The field dependence measured at 5 K shows a gradual increase in magnetization up to 55 000 G, although a decrease in the slope of the response is seen at fields greater than 20 000 G for both compounds. The measurements on all samples were conducted under increasing temperature (2−300 K) using a 500 G applied field. A diamagnetic correction was applied to the data to account for core diamagnetism. No correction was made for the diamagnetism of sample container because the measured moments of the compounds were over an order of magnitude larger.

Mössbauer Spectroscopy. Mössbauer spectra of $ErFe_4Al_9Si_6$ were taken between 18 and 300 K, in transmission geometry, using a constant acceleration spectrometer equipped with a $^{57}Co(Rh)$ source. The spectrometer was calibrated with α-Fe, and the isomer shift values are reported relative to this calibration. The experimental data were analyzed with a least-squares minimization routine using a sum of Lorentzian lines.

Thermal Gravimetric Analysis. A Shimadzu TGA-50 was used to perform thermal gravimetric analysis. Experiments were carried out in air (30 mL/min, Airgas); a low flow of nitrogen was added to protect the thermobalance (10 mL/min). The compressed air is ~21.5% O_2 in N_2; the experiments were therefore effectively conducted in a mix of 1:5.2 O_2 to N_2 atmosphere. Crystalline samples were handpicked for analysis and ranged from 12 to 32 mg. Samples were contained in fused-silica crucibles. The mass was monitored over the following heating cycle: 10 °C/min to 150 °C, 5 °C/min to 1000 °C, and an isothermal step at 1000 °C for 10 min. After 10 min at 1000 °C, the sample was allowed to cool to 25 °C, and then the heating cycle was performed again.

Results and Discussion

Synthesis. Tb or Er metal powder, iron, and silicon react in excess molten Al to form $REFe_4Al_9Si_6$ as small cubelike crystals. These facetted crystals can range from micrometer to several millimeters in size, often with several crystals growing together as a polycrystalline aggregate. Unlike in most cases when arc-melting and flux methods lead to different products,[9,11] arc-melting produces the same quaternary phase when excess Al is used. Arc-melted products

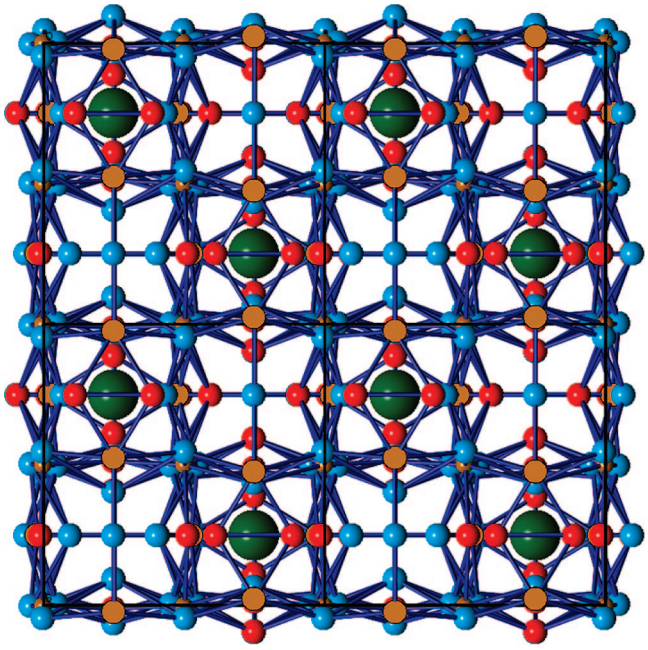

Figure 1. The tetragonal structure of $REFe_4Al_9Si_6$ (RE = Tb, Er) viewed down the *c*-axis. Green atoms, RE; large blue atoms, Al; red atoms, Si; brown atoms, Fe. The same coloring scheme is used in all figures.

form only as microcrystalline $REFe_4Al_9Si_6$ instead of large single crystals. Interestingly, when larger pieces of RE metal (>1 mm) were used as the starting material in Al flux, the reaction produced other phases, including $Tb_2Al_3Si_2$[13] and a variety of Fe/Al/Si phases. The reasons for this are not completely understood, but are likely because of differences in reaction kinetics that could affect the RE metal availability in the Al solution.

The $REFe_4Al_9Si_6$ phases appear to form predominantly with the late (smaller) rare earth metals, whereas the earlier rare earth metals tend to form phases of the $REFe_{2+x}Al_{7+x}Si_8$[11] type under similar reaction conditions. We also have preliminary experimental evidence that $REFe_4Al_9Si_6$ forms with Dy, Ho, Tm, and Yb.

Structural Description. The compounds $REFe_4Al_9Si_6$ (RE = Tb, Er) crystallize in the tetragonal space group $P4_2/nmc$ with the $NdRh_4Al_{15.4}$ structure type (see Figure 1). Up to now, the $NdRh_4Al_{15.4}$ structure type has been an "orphan" structure because of the lack of any reported phases that adopt it. The quaternary phases described here appear to be the first members to do so. Substantial deviations from the parent type exist because of ordering of atoms at the $z = 0$ plane, which in $NdRh_4Al_{15.4}$, are disordered. No disorder was found in $REFe_4Al_9Si_6$. The structure contains highly corrugated layers of merged cyclohexane-like Al_6 rings in the chair confirmation, shown in Figure 2a, b. These corrugated layers stack along the *c*-axis with the direction of the corrugation alternating along *a*- and *b*-axes respectively (Figure 3a). The rings consist of Al(1), Al(2), and Al(3) (Figure 3); the Al(4) atom sits between the corrugations of the layer, seen as the single nonbonded atom in Figure 3a.

When the Fe atoms are included in the framework, they occupy two positions in the structure. The first position is at the center of the Al_6 rings (see brown Fe atoms in Figure 2c), while the second is inserted between the corrugated layers (see the brown Fe atoms in Figure 3b). When the Si atoms are added in a subsequent step (Figure 3c), the non-rare-earth framework is complete. Finally, the RE atoms are added (Figure 3d) to complete the dense three-dimensional structure. There are Si−Si dimers in the structure with Si(3)−Si(3) bond length of 2.391(5) Å.

The RE atoms have a coordination number of 20 (6 Fe, 8 Al, and 6 Si), Figure 4. This coordination number is also found in rare earth atoms in the various structures including the compositions $RERe_2Al_{10}$ of the $CaCr_2Al_{10}$ structure type.[39,40] The coordination polyhedron of the rare earth atom is a 35-faced unit consisting of 33 trigonal and 2 square faces. A crystallographic mirror passes through the polyhedron and contains the RE atom.

Fe(1) has an unusual nine-coordinate arrangement that can be viewed as a sandwich of one five- membered and one four-membered Al/Si ring (Figure 5). Fe(2), on the other hand, is 10-coordinate that is best described as a sandwich between two five-membered rings in a ferrocene-like arrangement (Figure 5).

The Al and Si atoms in the structure exhibit a wide variety of coordination environments, as seen in Figure 6. Al(1) and Al(2) exhibit bicapped distorted trigonal pyramidal arrangements, whereas Al(3) exhibits a seven-coordinate hexagonal pyramidal arrangement. The atoms Si(2), Fe(2), Al(2), Fe(1), Al(2), and Fe(2) form the hexagonal base of the pyramid. The Al(4) atom exhibits a two-coordinate bent arrangement. The Si environments are irregular ranging from three-coordinate for Si(1) to five-coordinate environments for Si(2) and Si(3).

The stability of the $REFe_4Al_9Si_6$ stoichiometry in the $NdRh_4Al_{15.37}$ structure type[37] may be rationalized on the basis of its isoelectronic nature to the ternary aluminide. The substitution of Rh by Fe atoms in the structure creates an electron-poor environment that is then compensated by the replacement of some of the Al atoms with Si. The total valence electrons in the formula $NdRh_4Al_{15.37}$ is 85.11, which is very close to the 86 valence electrons in $REFe_4Al_9Si_6$ (for the purposes of this argument, we regard the f electrons to be core). If the electron count is normalized by the number of atoms in the formula, then the electron count is 4.33 e/atom in both cases. It would seem that this electron count favors this structure type and points to a possible explanation of the nonstoichiometry in $NdRh_4Al_{15.37}$. The full stoichiometry would be $NdRh_4Al_{16}$, which corresponds to a slightly more electron-rich state. Assuming the electron count dominates the stability of the structure and barring any steric effects, it is expected that the isoelectronic compounds $NdRh_uAl_{14}Si$ and $REMn_4Al_5Si_{10}$ are also stable.

Magnetism. Magnetic susceptibility measurements for $REFe_4Al_9Si_6$ (RE = Tb and Er) between 6 and 300 K show the compounds follow the Curie−Weiss Law (Figure 7). The calculated μ_{eff} for the Tb analogue was 10.36 μ_B with a Weiss constant of −17 K. The μ_{eff} value is close to the theoretical

(39) Fehrmann, B.; Jeitschko, W. *Zeitschrift Fur Naturforschung Section B-a Journal of Chemical Sciences* **1999**, *54* (10), 1277–1282.
(40) Cordier, G.; Czech, E.; Ochmann, H.; Schaefer, H. *J. Less-Common Met.* **1984**, *99*, 173–185.

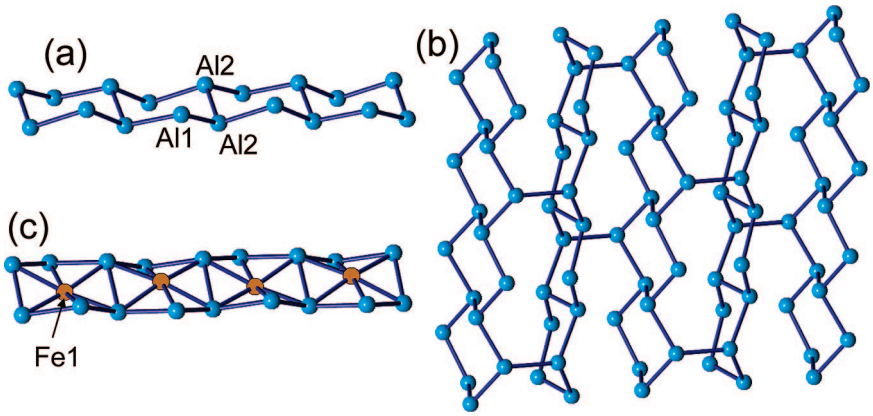

Figure 2. (a) A chain of fused cyclohexane-type Al_6 rings. (b) Slab of aluminum atoms made of a side-by-side association of chains. (c) Location of Fe1 atoms in the center of the cyclohexane-type Al_6 rings.

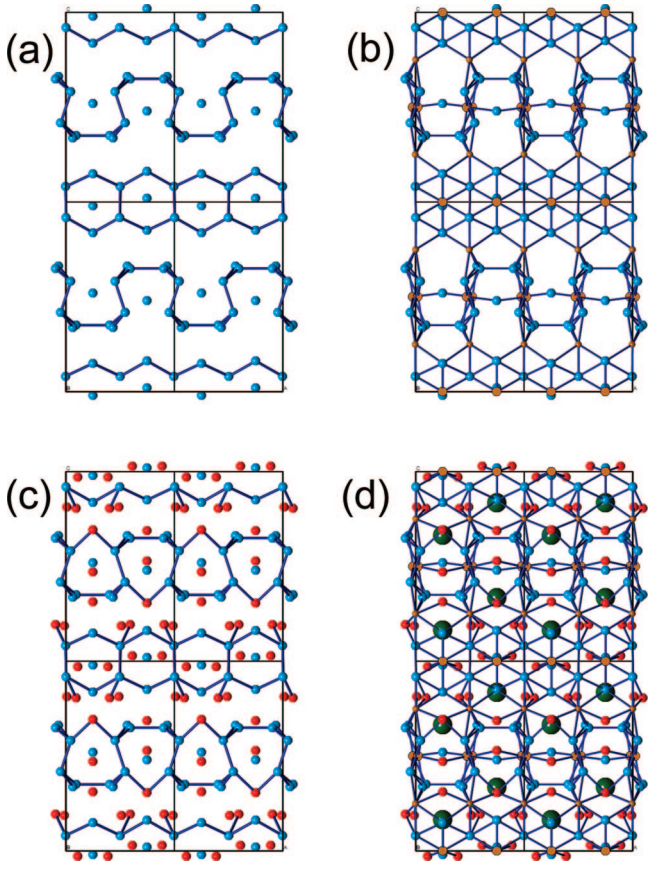

Figure 3. Structure of $REFe_4Al_9Si_6$ (RE = Tb, Er) shown built in stages as each element type is added. View down the *a*-axis. (a) Corrugated Al layers stacked along the *c*-axis with corrugation alternating between the *a* and *b* directions; (b) addition of the Fe atoms to the Al substructure; (c) insertion of Si atoms to the structure; and (d) finally, the RE atoms are added.

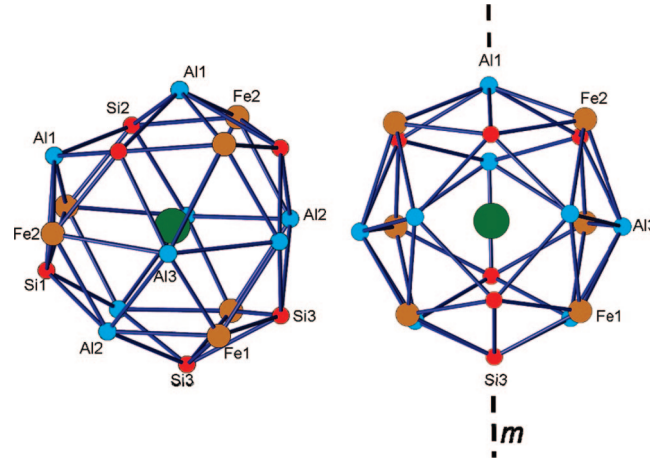

Figure 4. Two views of the local coordination environment of rare earth atom positions in $REFe_4Al_9Si_6$, drawn out to 3.5 Å. The coordination number of the RE atoms is 20. The dashed line passing through atoms Al1, RE, and Si3 represents crystallographic mirror symmetry.

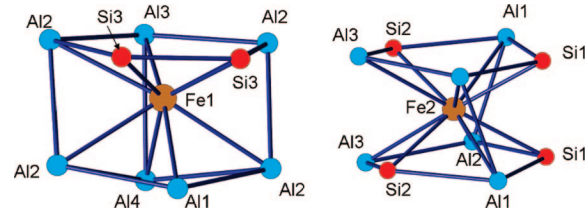

Figure 5. Local coordination environments of the Fe atoms positions in $REFe_4Al_9Si_6$ out to 3 Å. Bonds are drawn with interatomic distances out to 2.6 Å.

magnetic moment for Tb^{3+} of 9.72 μ_B[41] (Figure 7a), indicating that the Tb is in a 3+ state, whereas the Fe does not contribute to the overall magnetic susceptibility. No hysteresis is observed in the field dependent measurement for $TbFe_4Al_9Si_6$, as seen in Figure 7b. For $ErFe_4Al_9Si_6$, similar behavior was observed with a μ_{eff} of 10.03 μ_B, which is close to the expected Er^{3+} value of 9.74 μ_B (Figure 7a). The Weiss constant for the Er analogue was −22 K.

These properties are very similar to those of $RE_4Fe_{2+x}Al_6Si_{7-x}$.[11] Both types of compounds exhibit magnetism based predominantly on the rare earth element, with the Fe atoms not contributing to the overall magnetism. Although this is intriguing, given the relatively high atomic Fe/RE ratio in $REFe_4Al_9Si_6$, it has been observed in many ternary RE/Fe/Si compounds.[42,43] The diamagnetic behavior of Fe could be because of the filling of the d orbital bands induced by the excess of highly electropositive Al atoms (an essential chemical reduction) or because of strong spin-quenching hybridization effects between Fe/Si/Al orbitals.

(41) Bourdreaux, E. A.; Mulay, L. N. *Theory and Applications of Molecular Paramagnetism*; John Wiley and Sons: New York, 1976.

(42) Noakes, D. R.; Umarji, A. M.; Shenoy, G. K. *J. Magn. Magn. Mater.* **1983**, *39* (3), 309–316.

(43) Umarji, A. M.; Noakes, D. R.; Viccaro, P. J.; Shenoy, G. K.; Aldred, A. T.; Niarchos, D. *J. Magn. Magn. Mater.* **1983**, *36* (1−2), 61–65.

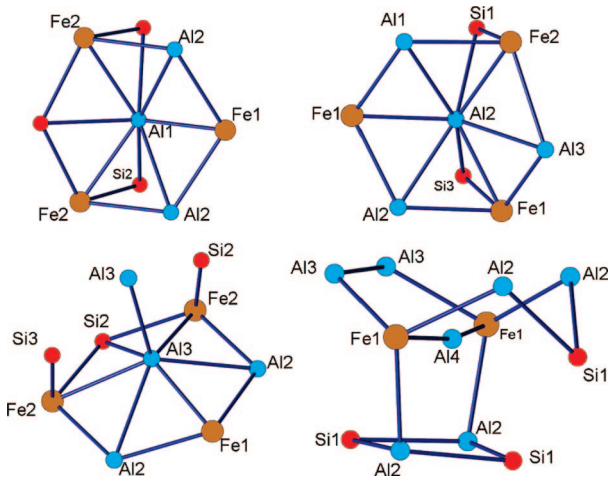

Figure 6. Local coordination environments of the Al atoms positions out to 3 Å. Bonds are drawn interatomic distances less than 2.6 Å for Fe−Si and Si−Si, 2.7 Å for Fe−Al and Si−Al, and 2.9 Å for Al−Al.

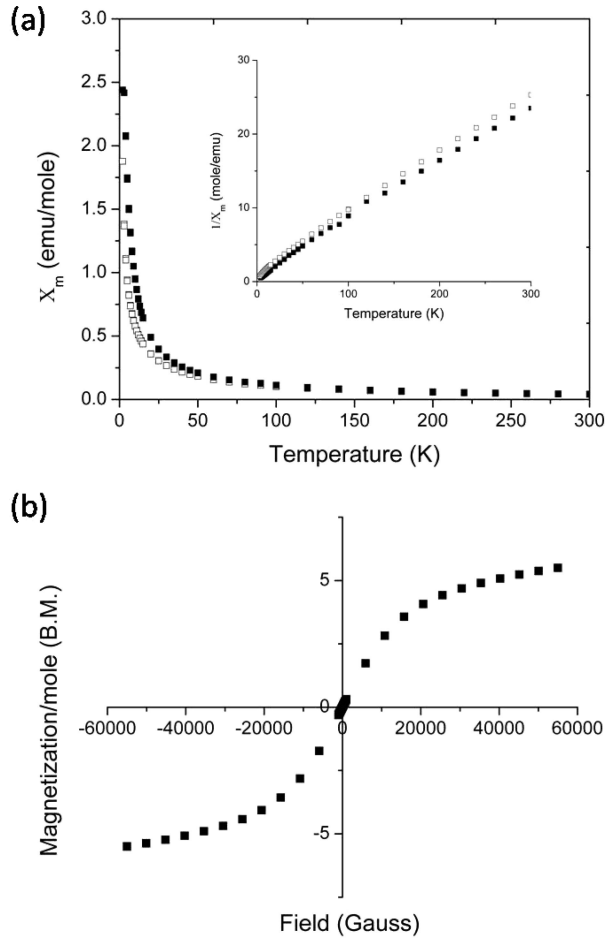

Figure 7. Temperature-dependent magnetic susceptibility data for (a) $TbFe_4Al_9Si_6$ (filled squares) and $ErFe_4Al_9Si_6$ (open squares). Insets show the dependence of inverse susceptibility for each compound. Field-dependent magnetization data for (b) $TbFe_4Al_9Si_6$.

Mössbauer Spectroscopy. To probe further the electronic state of iron in $REFe_4Al_9Si_6$ (RE = Tb, Er), we employed Mössbauer spectroscopy in the temperature region 18−300 K. The measured spectra profile for $ErFe_4Al_9Si_6$ did not change in the temperature range from 18 to 300K, and it can be analyzed with two superimposed paramagnetic doublets corresponding to the two independent Fe positions

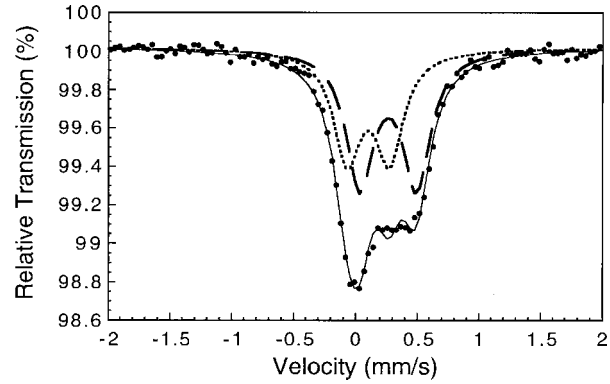

Figure 8. Mössbauer spectra of $ErFe_4Al_9Si_6$ taken at 18 K. The velocity corresponds to the isomer shift (IS), which is referenced to α-Fe.

Table 5. Mössbauer Parameters, Collected at 18 K for $ErFe_4Al_9Si_6$

	δ (mm/s)	ΔEq (mm/s)	$\Gamma/2$ (mm/s)	area (%)
site 1	0.37	0.46	0.13	56
site 2	0.21	0.34	0.13	44

in the structure. Figure 8 shows a typical spectrum taken at 18 K, and the hyperfine parameters are given in Table 5. The isomer shifts are centered at the positive values of 0.37 and 0.21 mm/s, showing again behavior similar to the previously reported values for $RE_4Fe_{2+x}Al_6Si_{7-x}$,[11] which exhibited a value of 0.21 mm/s for the single Fe position. The isomer shift values are also very close to those observed for other Fe/Si compounds and alloys[44] and suggest that the iron atoms are in a more reduced state relative to Fe metal. This means that there is a decrease in the s electron density on the Fe nucleus coming from either a decrease in the number of s electrons or an enhanced screening of the 4s electrons.[42,43] In other words, the Fe atoms seem to be more reduced than those in Fe metal, which is consistent with the expectation of d orbital-filling via electron transfer from the electropositive RE and Al atoms. This electron flow direction is reasonable because the Fe atoms are more electronegative than RE and Al. There was no evidence for magnetic ordering of Fe atoms seen in the Mössbauer spectra, as expected due to the relatively large Fe−Fe distances (4.364(1) Å).

Thermal Stability and Oxidation Resistance. Many intermetallic alloys are of interest for use in high-temperature processes, such as steel making, heat treating, and chemical processing, because of their corrosion and oxidation resistance at these extreme temperatures.[45] Heat-resistant alloys depend on the formation of protective oxide scales on the metal surface to inhibit decomposition by oxidation. Protective oxide coatings can fail via exfoliation or spallation from the metal surface. The reactive element effect, adding reactive elements such as rare earths or their oxides to the alloy, is often used to enhance the thermal stability by forming a layer between the protective oxide and the bulk to both increase adhesion of the oxide layer and decrease the rate of oxygen diffusion into the bulk.[46,47] Little, however, is known about

(44) Noakes, D. R.; Shenoy, G. K.; Niarchos, D.; Umarji, A. M.; Aldred, A. T. *Phys. Rev. B* **1983**, *27* (7), 4317–4324.
(45) Stoloff, N. S.; Liu, C. T.; Deevi, S. C. *Intermetallics* **2000**, *8*, 1313–1320.

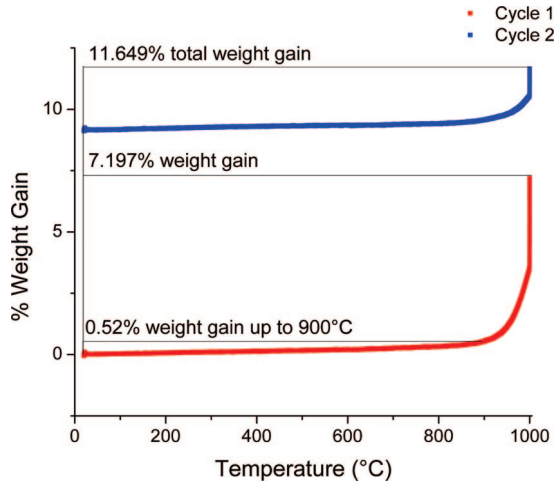

Figure 9. Thermal gravimetric analysis curve of crystals of $TbFe_4Al_9Si_6$.

the chemistry occurring at the interfaces that can bring about the enhanced thermal stability to explain this effect. The oxidation resistance of rare-earth-containing intermetallics should be investigated to help understand what is happening in the alloys or to identify new high-temperature oxidation-resistant materials. $Tm_5Co_4Si_{14}$, for example, shows remarkable resistance to oxidation up to 1000 °C, with different scale formations on dissimilar faces of the single crystals.[29] We find similar behavior in $TbFe_4Al_9Si_6$.

The oxidation resistance of single crystals of $TbFe_4Al_9Si_6$ was investigated with thermal gravimetric analysis (TGA) under flowing air (Figure 9). If $TbFe_4Al_9Si_6$ were to completely oxidize into the highest oxidation state oxide binaries (Tb_2O_3, Fe_2O_3, Al_2O_3, and SiO_2), the compound could theoretically have a 66.53% weight gain. The $TbFe_4Al_9Si_6$ crystals showed excellent resistance to oxidation up to 900 °C with only up to 0.52% weight gain. This is better than the 3% weight gain observed for $Co_5Al_{14}Si_2$ up to 900 °C[18] and comparable to the 1% weight gain observed for $Tm_5Co_4Si_{14}$ up to 1000 °C.[29]

Above 900 °C, the $TbFe_4Al_9Si_6$ crystals began to oxidize more rapidly. During the first heating cycle, the isothermal heating at 1000 °C of $TbFe_4Al_9Si_6$ exhibited a weight gain rate of 1.32×10^{-3} mg/s. The same sample of $TbFe_4Al_9Si_6$ was cooled and subjected to a second heating cycle in the TGA. The weight gain rate during the second isothermal heating at 1000 °C was decreased by almost an order of magnitude to 3.94×10^{-4} mg/s. This clearly shows that the protective oxide scale grown in the first heating cycle decreases the rate of oxygen diffusion into the bulk $TbFe_4Al_9Si_6$ and must remain relatively resistant to exfoliation and spallation effects.

Scanning electron micrograph images of $TbFe_4Al_9Si_6$ show the crystals before heating and the scale formations found on different faces of a crystal after heating (Figure 10). Before the crystals are heated, they appear well-defined with flat faces (Figure 10a). After being heated in air, the crystals retain their shapes with oxide scale on the surface (Figure 10b). The scale that grows on the (100) face appears as a smooth crust (Figure 10c), but the scale on the (−110) face has needles and pyramids growing from the surface (Figure

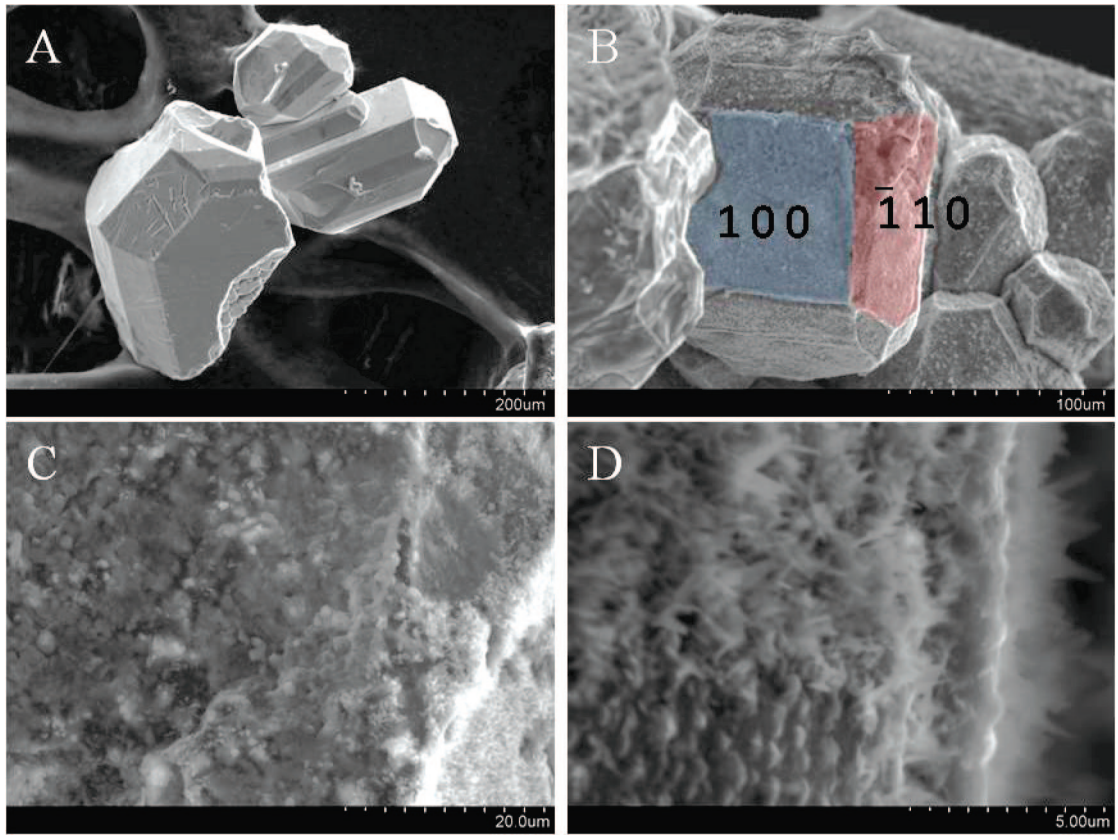

Figure 10. Scanning electron micrographs of $TbFe_4Al_9Si_6$ crystals: (a) as prepared $TbFe_4Al_9Si_6$ single crystals, (b) crystals after heating in air in the TGA to 1000 °C, (c) oxide scale formation on the (100) face of the crystal after heating, and (d) oxide scale formation on the (−110) face showing needles and pyramids.

10d). EDS analysis of the needles and pyramids growing from the (−110) face consisted of a combination of alumina and silica with a 4:1 atomic ratio of Al/Si. It is likely that the pyramids are the base of alumina/silica crystal growth on the surface and that the needles have been exfoliated from the surface in these locations. The EDS analysis of the smooth crust on the (100) face shows an increase in Fe concentration and a decrease Si concentration with a 8:1:1 atomic ratio of Al/Fe/Si.

The difference in scale formation can be understood when the chemical composition of the planes parallel to the faces is considered. The interplanar distance between Tb-containing planes parallel to the (100) face is approximately 4.2 Å. For Tb-containing planes parallel to the (−110), the interplanar distance is much longer, about 6.4 Å. As the compound oxidizes, the Tb atoms can migrate more readily to the (100) surface than the (−110) surface because they have to travel a shorter distance. The complex Tb metal oxide coating under the alumina and silica is thus thicker on the (100) surface and creates a stronger barrier to oxygen diffusion as well as stronger adhesion of the scale to the surface. This is an example of the reactive element effect[46,47] occurring within a single crystalline environment.

Concluding Remarks. The new compounds $REFe_4Al_9Si_6$ (RE = Tb, Er) form readily in liquid Al. The structure is an ordered variant of the $NdRh_4Al_{15.4}$ structure type. The nonstoichiometry of the latter is not observed in the quaternary compounds because the $REFe_4Al_9Si_6$ is, in fact, isoelectronic to it. The RE atoms exhibit behavior typical of a 3+ oxidation state, whereas the Fe atoms appear to be magnetically silent. This result is particularly interesting in conjunction with the results of Mössbauer spectroscopy that show the Fe atoms to be more reduced than those in Fe metal. The discovery of compounds with high stoichiometric complexity underscores the difficulties associated with trying to predict them and the importance of and opportunities available with molten metal fluxes in exploratory materials synthesis.

There are links between the synthetic work described here and the metallurgical studies of aluminum alloys. Iron-rich intermetallic phases are well-known to strongly influence the mechanical properties of Al−Si alloys. The phase often identified as having a detrimental effect is the tetragonal $FeAl_3Si_2$.[48] The results described here and the discovery of $REFe_4Al_9Si_6$ phases point to the proposition that the addition of RE atoms in Fe/Si/Al mixtures may help suppress the formation of $FeAl_3Si_2$ by forming potentially less harmful quaternary phases.

When choosing a material for high-temperature applications, both the mechanical properties and oxidation resistance must be considered. As well as improving the mechanical properties of Fe/Si/Al alloys, the addition of RE atoms to Fe/Si/Al mixtures plays a crucial role in increasing the oxidation resistance of the material at high temperatures via the reactive element effect. $REFe_4Al_9Si_6$ represents a complex intermetallic phase resistant to oxidation up to 900 °C. Other complex RE/M/Al/Si phases may prove a fertile source of oxidation resistant intermetallic materials.

Acknowledgment. Financial support from the Department of Energy (Grant DE-FG02-07ER46356, Northwestern University) is gratefully acknowledged. The work at Argonne National Laboratory (IPNS) was supported by the U.S. Department of Energy, Basic Energy Sciences-Materials Sciences, under Contract No. W-31-109-ENG-38.

Supporting Information Available: Additional experimental details and crystallographic data. This material is available free of charge via the Internet at http://pubs.acs.org.

CM801554D

(46) Stringer, J. *Mater. Sci. Eng., A* **1989**, *120*, 129–137.
(47) Whittle, D. P.; J., S. *Philos. Trans. R. Soc. London, A* **1980**, *295*, 309–329.
(48) Kral, M. V. *Mater. Lett.* **2005**, *59* (18), 2271–2276.